Measurement of the decay rate for the process $K_L^0 \to \mu^+\mu^-$

M. J. Shochet, P. Linsay,* C. Grosso-Pilcher, H. J. Frisch, R. DeVoe,† and J. W. Cronin
Enrico Fermi Institute and Department of Physics, University of Chicago, Chicago, Illinois 60637

D. R. Moffett
Argonne National Laboratory, Argonne, Illinois 60439
(Received 30 November 1978)

The branching ratio $\Gamma(K_L^0 \to \mu^+\mu^-)/\Gamma(K_L^0 \to \pi^+\pi^-)$ has been measured and found to be $4.0^{+1.4}_{-0.9} \times 10^{-6}$. With the same apparatus the branching ratio $\Gamma(K_L^0 \to \pi^+\pi^-)/\Gamma(K_L^0 \to \text{all})$ has been measured to be $(2.01 \pm 0.09) \times 10^{-3}$. The combination of these two results gives $\Gamma(K_L^0 \to \mu^+\mu^-)/\Gamma(K_L^0 \to \text{all}) = 8.1^{+2.8}_{-1.8} \times 10^{-9}$. This result is consistent with the lower bound predicted from the decay rate $K_L \to \gamma\gamma$ and unitarity.

I. INTRODUCTION

The decay mode $K_L \to \mu^+\mu^-$ has been of great interest in recent years. Originally the interest centered around the fact that $K_L \to \mu^+\mu^-$ when mediated by a purely weak interaction would be an example of a strangeness-changing neutral-current interaction. Early measurements of this decay mode were made as by-products of studies of CP violation in K_L^0 decay and produced only upper limits.[1,2]

Early it was realized that the requirements of unitarity and quantum electrodynamics gave a lower limit to the decay rate of a pseudoscalar particle into two muons in terms of its decay rate into two photons.[3,4] Subsequently, specific application of these ideas was made to K_L^0 decay[5-7] with the result that

$$\Gamma(K_L \to \mu^+\mu^-)/\Gamma(K_L \to \gamma\gamma) \geq 1.2 \times 10^{-5}.$$

With the world average[8] for the branching ratio

$$\Gamma(K_L \to \gamma\gamma)/\Gamma(K_L \to \text{all}) = (4.9 \pm 0.5) \times 10^{-4},$$

one expected

$$R_{\mu\mu} = \Gamma(K_L \to \mu^+\mu^-)/\Gamma(K_L \to \text{all}) \geq (5.9 \pm 0.6) \times 10^{-9}.$$

In an experiment at Berkeley dedicated to the measurement of $K_L \to \mu^+\mu^-$, Clark *et al.*[9] found $R_{\mu\mu} \leq 1.8 \times 10^{-9}$ with 90% confidence. This result not only gave a very low limit for weak strangeness-changing neutral currents, but also violated the unitarity limit mentioned above. This violation called into question physics principles with very sound foundations (unitarity, quantum electrodynamics, and CPT conservation). A large amount of theoretical effort was invested to understand the low value of $R_{\mu\mu}$ while preserving the aforementioned principles. These efforts, which were unsuccessful in reconciling the experimental result with the theory, were reviewed by Stern and Gaillard[10] and Dolgov, Okun, and Zakharov,[11] and the reader is directed to these references for an excellent discussion of the $K_L \to \mu^+\mu^-$ puzzle.

Two subsequent measurements have shown a positive effect. Carithers *et al.*[12] observed nine events giving $R_{\mu\mu} = 12^{+8}_{-4} \times 10^{-9}$ (90% confidence level) and Fukushima *et al.*[13] observed three events giving $R_{\mu\mu} = 9^{+11}_{-6} \times 10^{-9}$. The present experiment was carried out with significantly higher sensitivity and improved background rejection to resolve any remaining doubt that the $K_L \to \mu^+\mu^-$ decay mode exists and does not violate the unitarity bound.

As with all measurements of $R_{\mu\mu}$, the quantity actually measured was $\Gamma(K_L \to \mu^+\mu^-)/\Gamma(K_L \to \pi^+\pi^-)$. This was done because the CP-violating $K_L \to \pi^+\pi^-$ decays are kinematically almost identical to the dimuon decays. In order to obtain $R_{\mu\mu}$, the ratio $\Gamma(K_L \to \pi^+\pi^-)/\Gamma(K_L \to \text{all})$ must be known. The accepted value of this quantity has undergone significant changes recently because of new measurements. In order to make our measurement of $R_{\mu\mu}$ self-contained, we have also measured the ratio $\Gamma(K_L \to \pi^+\pi^-)/\Gamma(K_L \to \text{all})$ with the same apparatus. Brief reports of this work have already been published.[14,15]

The apparatus is described in Sec. II. The data analysis is presented in Sec. III. In Sec. IV the Monte Carlo calculation of the relative detection efficiencies for $K_L \to \mu^+\mu^-$ and $K_L \to \pi^+\pi^-$ is described. The results for the $\Gamma(K_L \to \mu^+\mu^-)/\Gamma(K_L \to \pi^+\pi^-)$ measurement and comparison with other experiments are presented in Sec. V.

II. APPARATUS

A. Beam

The experiment was performed in a high-intensity K_L beam at the Argonne Zero Gradient Synchrotron (ZGS). The beam, shown schematically in Fig. 1, was produced by 12-GeV/c protons striking a 1.27-cm-wide × 1.90-cm-high × 10.16-cm-long Cu target. The neutral beam was produced at 4° and was defined by two collimators, each preceded by a sweeping magnet. The collimator system accepted a 35-mrad vertical aperture and 20-mrad horizontal aperture giving a total solid angle of 0.7 msr. The beam collimation system was 6.0 m in length and was followed by a 10.4-m-long vacuum tank. At the end of the tank a thin window 0.76-m-high × 2.54-m-long was placed. The window was constructed from a 127-μ-thick Mylar sheet supported by dacron sailcloth of thickness 0.04 g/cm^2.

The characteristics of the beam were estimated from a charged-K-meson beam produced at the same angle[16] at the ZGS. For a typical pulse of 2.5×10^{11} protons striking the target, approximately 10^6 K_L mesons with momenta between 2 and 7 GeV/c decayed in the vacuum tank. The beam intensity was monitored by two counter telescopes. One, consisting of three scintillators, viewed the target through a hole in the shielding at an angle of 90° with respect to the beam. The other, consisting of two scintillators, was located in the neutral beam at the entrance to the beam dump.

B. Spectrometer

The K_L decay products were analyzed in a double-arm spectrometer shown schematically in Fig. 2. It was designed to have large acceptance and good background rejection. The large acceptance was achieved by constructing large-aperture magnets (1.00 m wide × 0.86 m high). Each magnet was capable of giving a 0.112-GeV/c transverse kick to a charged particle. Each arm of the spectrometer contained two magnets so that the momentum of a charged particle passing through the magnets could be effectively measured twice.

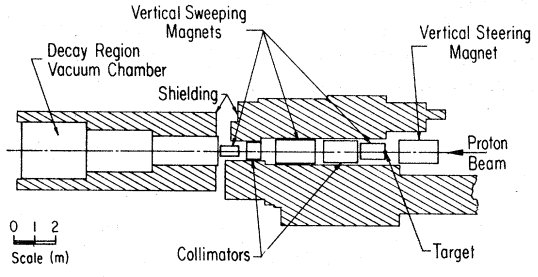

FIG. 1. Schematic view of the neutral beam.

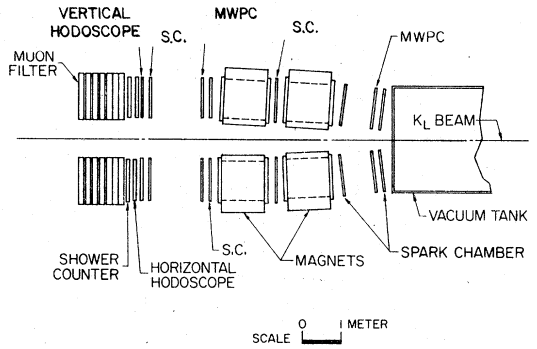

FIG. 2. Schematic view of the apparatus.

The principal background in the $K_L \to \mu^+\mu^-$ measurement comes from $K_L \to \pi\mu\nu$ decays in which the π decays to a μ in the middle of the spectrometer in such a way that the effective mass lies under the $K_L \to \mu^+\mu^-$ mass peak. Suppression of this background is more effective in a double magnet system since the π-μ decay is marked by a correlated change in angle and momentum. Those $K_L \to \pi\mu\nu$ decays which lead to a background are strongly suppressed by the requirement that each decay track has a smooth trajectory through both magnets.

The magnetic field of the spectrometer including the relevant fringe fields was measured with a calibrated flip coil in a grid of 2.54-cm vertical steps, 5.08-cm horizontal steps, and 2.54-cm steps along the beam. These measurements were converted to a map of field integrals which was used to determine the momentum of each track detected in the spectrometer. Stability of the overall normalization of the field was obtained by powering the four magnets in series and recording the current after each beam pulse.

The particle trajectory in each arm was measured with five double-gap wire spark chambers. Each chamber was 1 m × 1 m and was constructed with 76-μ-diameter Al wires to minimize multiple scattering. The wire spacing was 1.06 mm. The windows of the chambers were made of 25-μ aluminized Mylar. Two measurements each of the horizontal and vertical coordinates were made by reading out both low-voltage and high-voltage planes. A high overall efficiency for the spark-chamber system was achieved by the requirement that only one of the two possible gaps need fire.

The spark positions were determined by reading out capacitors attached to each wire using a parallel-input serial-output shift-register system. A detailed description of this spark-chamber data-

acquisition system has been given by its developer, Nunamaker.[17] This system was sensitive to very-low-current sparks thus providing a very high multitrack efficiency.

The trigger elements consisted of scintillation counters and multiwire proportional chambers (MWPC's). In each arm of the spectrometer an MWPC was placed immediately behind the forward spark chamber (see Fig. 2). An MWPC was also placed behind the fourth spark chamber, just downstream of the magnet. Vertical and horizontal scintillation hodoscopes were placed behind the final spark chamber immediately before the particle identification system.

Each MWPC was 1 m wide $\times$0.8 m high with a single plane of vertical wires spaced 3.15 mm apart. Four wires were attached to a single amplifier so that each MWPC was effectively a vertical hodoscope with 80 elements each 1.25 cm wide. The forward MWPC's were normally not used in the trigger, but served as markers for the location of the proper spark in the adjacent spark chamber. The time resolution of the MWPC was 100 nsec which was 10 times less than the sensitive time of the spark chambers.

The horizontal scintillation hodoscope consisted of 21 vertical 1.01-m-long $\times$ 7.62-cm-wide plastic counters which were overlapped to form 40 channels each 2.54 cm wide. Vertical information was obtained with six scintillation counters each 19.0 cm high by 1.01 m wide.

Immediately downstream of the hodoscope, a particle identifier was placed. The particle identifier provided crude muon range information and rejection of pions and electrons. The first element of the identifier was a liquid scintillation shower counter. The counter was 122 cm high by 122 cm wide and contained eleven lead sheets comprising six radiation lengths. These counters provided excellent muon-electron separation. Although it proved unnecessary to use this counter information to select the final dimuon sample, it was very useful in identifying samples of $K\mu_3$ and $K\pi_2$ decay for various calibrations.

The muon detectors consisted of four banks of scintillation counters separated by blocks of steel. The muon ranges at these banks corresponded to momenta of approximately 850, 1050, 1250, and 1450 MeV/c. These momenta were obtained both from calculations of energy loss and from samples of muons whose momenta were measured in the magnetic spectrometer. The scintillator banks each contained four 30.5-cm $\times$ 122-cm counters arranged such that vertical position information was obtained in the first and third banks, with the second and fourth banks providing horizontal position information. This allowed us to crudely check that a particle in the muon detector lay along the trajectory measured in the spectrometer.

Great care was taken to minimize the effects of multiple scattering. For example, scintillation counters were encountered by a particle only after it had completely passed through the spectrometer. The total amount of material in the spectrometer and vacuum tank window corresponded to 0.009 radiation lengths.

The apparatus was triggered in two modes: one for the detection of $K^0_L \to \mu^+\mu^-$ events, the other for the detection of the $K^0_L \to \pi^+\pi^-$ normalization events. In both cases each of the two tracks was required to be deflected in the magnets so that upon exit the particle was approximately parallel to the K^0_L beam line. Since the magnets imparted a transverse momentum kick of $\approx$225 MeV/c to a particle, the parallel condition was only satisfied if both particles had transverse momenta $\approx$225 MeV/c at the entrance to the spectrometer. The requirement was met by most two-body K^0_L decays, while for the three-body leptonic decays, it was only satisfied in the corner of the Dalitz plot where the neutrino carried off little energy.

The parallel condition was established by a pair of hardware coincidence matrices which operated on the signals from the downstream multiwire proportional chambers and horizontal hodoscopes. Although the width of the angular requirement could be varied, it was set during the data taking so that each track was required to bend toward the beam line with an angle less than 33 mrad or bend away from the beam line with an angle less than 25 mrad. Without the parallel requirement, the relative three-body (leptonic) to two-body acceptance was 0.3; with the matrices in the trigger this was reduced to 0.05.

The $K^0_L \to \mu^+\mu^-$ trigger required that each particle satisfy the parallel condition in coincidence with signals from the vertical hodoscope, the first muon counter bank, and the second muon counter bank. Normalization data ($K^0_L \to \pi^+\pi^-$) were taken every sixteenth accelerator pulse by removing the muon counters from the trigger. The beam monitors, which were gated along with the rest of the apparatus, recorded the relative exposures for the normalization and $\mu^+\mu^-$ data.

A number of checks were made to determine if there were systematic biases between the two sets of data ($\pi\pi$ and $\mu\mu$ triggers). In one such test we measured the numbers of reconstructed events in a particular kinematic region for which both tracks were muons. If the operating conditions (e.g., spark-chamber efficiency) for the two trigger modes were the same, then the rates for these events when normalized to the beam monitor would be equal. The ratio of the rates was 1.0 ± 0.05.

Extreme care had to be taken to ensure that the muon trigger was efficient. Consideration of this efficiency had two aspects. One was the electronic efficiency and the second was the detection efficiency which is somewhat less than unity because of cracks between scintillation counters and range straggling of the stopping muons. With regard to the first condition, the $\mu\mu$ trigger pulse was latched during all the normalization runs. (The latching efficiency was 100%.) Then in subsequent analysis of the normalizing data, those events which satisfied the muon requirement as determined by muon counter pulse heights were compared with those which possessed a muon latch. Those with a muon latch would have triggered, had the trigger been set in the $\mu^+\mu^-$ mode. The electronic efficiency was $97.5\% \pm 1.0\%$.

C. Data acquisition

Information on each event was transferred via a CAMAC interface into a PDP 11/45 computer on-line. The computer was used both to monitor the performance of the apparatus and to record the data on magnetic tape for off-line analysis.

For each trigger, latches on the muon counters and vertical hodoscope counters were recorded along with the pulse heights of shower counters and muon counters. Latches for the horizontal hodoscope and the MWPC wires were transferred to the computer via a scanner and shift-register readout.[17] Finally, the spark-chamber information was transferred.

A dead time of ~5 msec was introduced for the apparatus to permit the transfer of the data (~2 msec) and the recharging of the spark-chamber capacitors (~5 msec). The beam monitors and other scaled quantities were also gated off during this period. At the end of the accelerator pulse, which lasted ~350 msec, the scalers and magnet currents were read into the computer.

Between accelerator pulses the data were written on magnetic tape and an on-line program checked for the presence of spark-chamber fiducials to ensure the integrity of the shift-register lines. Also, data were accumulated into histograms for different elements of the apparatus and displayed between accelerator pulses. A simplified pattern-recognition program searched for tracks and calculated the efficiency of each of the 40 spark-chamber planes.

Typical event rates were ~7/pulse for the $\mu^+\mu^-$ trigger and 40/pulse for the $\pi^+\pi^-$ trigger, the latter being dead-time–limited.

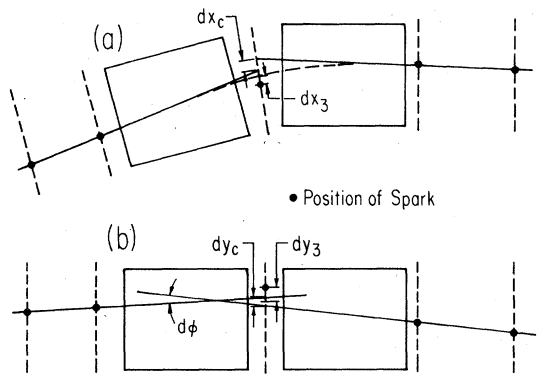

FIG. 3. (a) Variables used in constructing the χ^2 for the horizontal plane. (b) Variables used in constructing the χ^2 for the vertical plane.

III. DATA ANALYSIS

A. Spatial reconstruction

The data were reduced by a two-pass process. In the first pass the spatial reconstruction was carried out with rather loose demands of orbit continuity through the full spectrometer. In a second pass, using the summary tapes produced in the first pass, detailed evaluation of the orbits was used to remove the $K_L \to \pi\mu\nu$ background.

The events were spatially reconstructed off-line on an IBM 370/195 computer. The pattern-recognition program was designed for high reconstruction efficiency. The counter-hodoscope and MWPC information was used to define roads in the spark chambers in which to search for sparks. The upstream MWPC's were particularly important in this regard since the multiplicity in the forward spark chambers was about 8.

Because of this high multiplicity the track search was started in the rear chambers, both in the horizontal and vertical planes. The information from the rear segments was used to predict the track position in the front of the apparatus. To obtain a high reconstruction efficiency, only one spark per double-gap chamber was required.

Simple selection criteria were defined to locate the projection of the track in the horizontal and vertical views. In the horizontal plane a χ^2 was calculated to express the goodness of fit of a set of five sparks to a smooth circular trajectory through the magnets. (The standard deviations appropriate to the χ^2 calculation were obtained from a study of the data.) There were two degrees of freedom for this calculation. For the vertical view, since the vertical focusing was small, a χ^2 was calculated that the five sparks lay on a straight line. If only one track solution was possible, then the event was kept regardless of the quality of fit.

The response of the program for multiple solutions was more complex. In many cases there

were extra sparks. Any given spark was not eliminated as a candidate for another possible track even though that spark may have been successfully used in a given track solution. Further, if in using the counter hodoscope and MWPC information no track was found, the search program was reinitiated ignoring the information. If the MWPC information upstream was missing (because it had a small inefficiency), the program searched for tracks without that information.

In the case of multiple solutions for a track, the solutions were ordered according to the χ^2. The best solution was kept and any additional solutions for which the χ^2 was less than 10 (12) in the horizontal plane (vertical plane) were kept. In a given arm the average multiplicity of solutions was 1.6.

For each track the momentum was calculated from the deflection in the magnets. For each track pair a vertex and a distance of closest approach in the vacuum chamber were calculated, and a very loose cut was imposed on the latter quantity. The K_L momentum, the 2μ or 2π invariant mass, and the angle α between the vector momentum sum of the two tracks and the original K_L direction were also calculated.

All of this information along with the original coordinates of the tracks, and all counter and MWPC information were recorded on a secondary tape. From these tapes events with $480 < M_K < 530$ MeV/c^2 and $\alpha^2 < 100$ mrad^2 were placed on a tertiary tape for detailed analysis, which was carried out on the PDP 11/45.

B. Selection of $K_L \to \mu^+\mu^-$ events

The major background in a search for $K_L^0 \to \mu^+\mu^-$ events comes from $K_L^0 \to \pi\mu\nu$ in which the π decays in flight into $\mu\nu$. A large suppression of this background can be obtained if one can detect the track discontinuity which occurs when the π decays. We thus calculate for each track a χ^2 for the hypothesis that the sparks in the chambers lie along a continuous particle trajectory. We use the data to measure all the standard deviations that are involved in the χ^2 procedure.

The χ^2 in the horizontal plane has two degrees of freedom [see Fig. 3(a)] since five measured coordinates are used to obtain the position and angle of the track at the entrance to the spectrometer as well as the particle's momentum. The variables chosen to characterize these degrees of freedom are (1) dx_c, the separation at the center of the spectrometer between the extrapolated tracks from before and after the magnets, and (2) dx_3, the difference between the measured and predicted position of the spark in the center chamber. The predicted position in the central chamber is obtained from the continuous particle trajectory which passes through the sparks in the other chambers.

The χ^2 in the vertical plane has three degrees of freedom since there is no momentum measurement in this view [see Fig. 3(b)]. The variables, (1) dy_c and (2) dy_3, are similar to dx_c and dx_3 in the horizontal view. The third variable, $d\phi$, is the angle between the trajectories before and after the magnets. The angle is calculated after a correction is made for vertical edge focusing in the magnets.

A sample of 20 000 $K_L^0 \to \pi^+\pi^-$ decays was used to develop the χ^2 procedure. These events consisted of normalization ($\pi\pi$) triggers in which the signals from the shower counters and muon counters showed that neither particle was a muon or an electron. The values of M_K and α were restricted to the region of the $K_L^0 \to \pi^+\pi^-$ peak, resulting in a sample with $< 1\%$ background contamination. These events were then used to study the dependence of

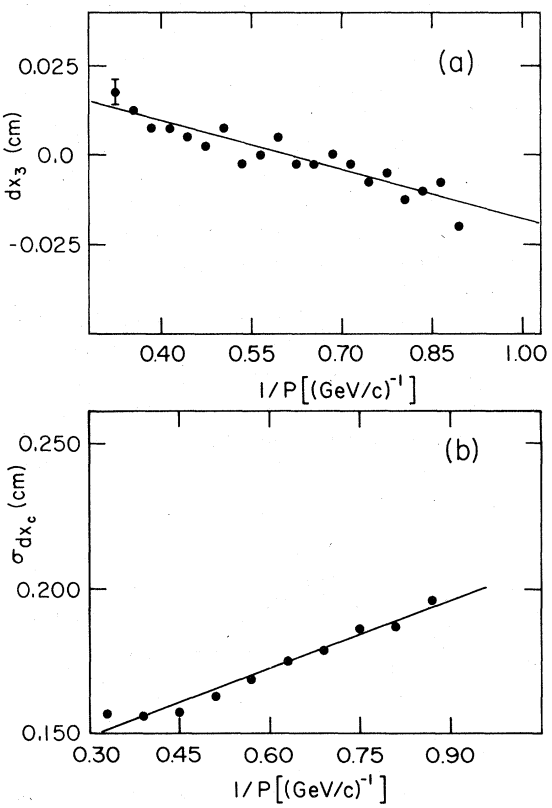

FIG. 4. (a) dx_3 as a function of the reciprocal of the momentum. The systematic effect due to the small nonuniformity in the magnetic field was removed by making an empirical correction to dx_3 shown as the line in the figure. (b) Standard deviation of dx_c as a function of the reciprocal of the momentum.

TABLE I. Standard deviations of the χ^2 variables determined from $K_L \to \pi\pi$ data with track momenta of 2 GeV/c.

Variable	Standard deviation
dx_c	1.72 mm
dx_3	0.71 mm
dy_c	1.52 mm
dy_x	0.96 mm
$d\phi$	0.95 mrad

each χ^2 variable on the track momentum as well as on the vertical and horizontal track positions. Systematic effects such as the one shown in Fig. 4(a) existed because of small nonuniformities in the magnetic field. Measurements of the magnetic field, when reduced to a table of field integrals, were sufficient to calculate particle momentum. The field integrals were not sufficient, however, for obtaining the precise trajectory through the magnetic field. The sample of $K^0_L \to \pi^+\pi^-$ events with trajectories known to be continuous allowed us to make empirical corrections to the χ^2 variables, thus removing the effects of the field nonuniformities.

The standard deviations for the χ^2 variables were also determined from this data sample. They were a function of the particle momentum; an example is shown in Fig. 4(b). The standard deviations for a track momentum of 2 GeV/c are given in Table I.

The horizontal and vertical error matrices were then orthogonalized, with χ^2_x and χ^2_y being calculated as the sum of the squares of these orthonormal variables. Distributions of χ^2_x and χ^2_y for the sample of 20 000 $K^0_L \to \pi^+\pi^-$ events are shown in Fig. 5. Also shown are ideal χ^2 distributions for two and three degrees of freedom. The empirical correction procedure reduced an initially large tail on the χ^2 distribution to the insignificant tail in the figures.

The χ^2 was also used in this second pass of the reconstruction program to select the sparks on the trajectory when there were a number of sparks close enough to each other so that multiple solutions were possible in the first pass. The success of the selection procedure can be seen in Fig. 6 which shows the χ^2 distribution for a sample of

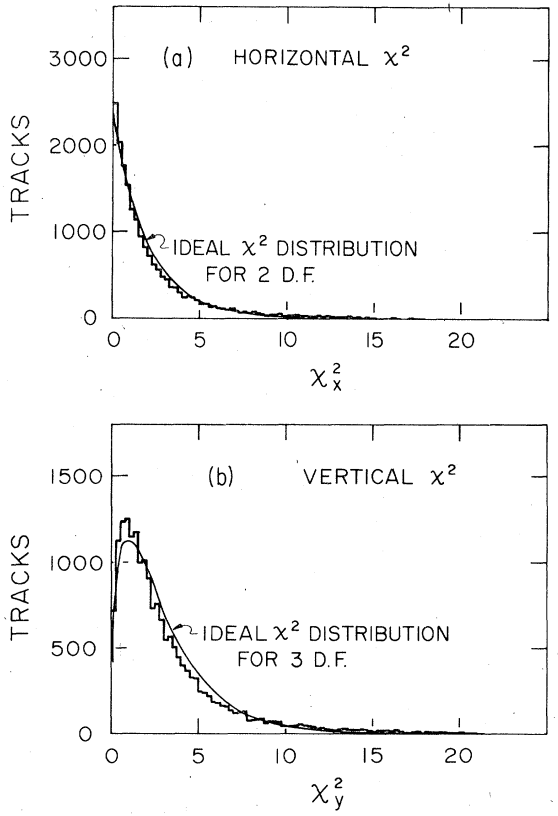

FIG. 5. (a) χ^2 distribution in the horizontal view for selected $K_L \to \pi\pi$ events (events with known continuous particle trajectories). (b) χ^2 distribution in the vertical view for the selected $K_L \to \pi\pi$ events.

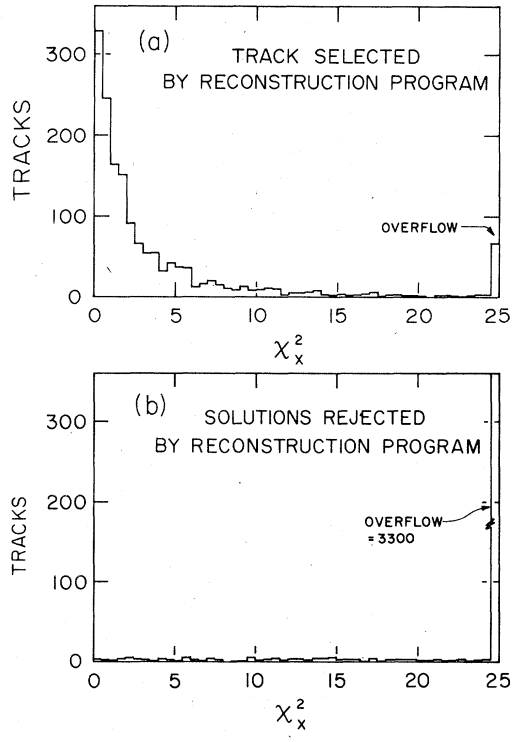

FIG. 6. (a) $\chi_x{}^2$ distribution for events selected in the second pass. (b) $\chi_x{}^2$ distribution for solutions rejected in the second pass.

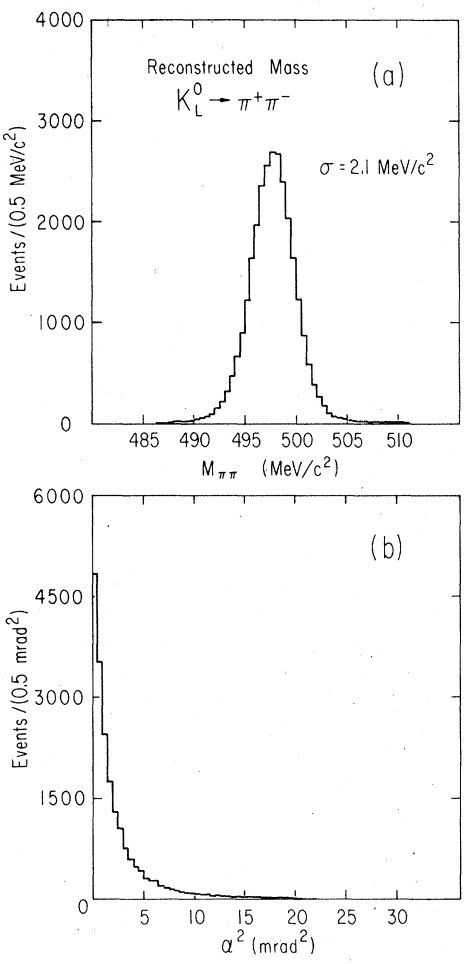

FIG. 7. (a) Mass distribution of selected $K_L \to \pi^+\pi^-$ events showing invariant-mass resolution. (b) Distribution of angles α for selected $K_L \to \pi^+\pi^-$ events.

events which have multiple solutions. Figure 6(a) is the χ^2 distribution for the selected tracks, while Fig. 6(b) is the χ^2 distribution for the rejected solutions. The χ^2 is sufficiently sensitive so that there is little ambiguity in the selection. One notes that there is no peak at low χ^2 for the rejected solutions.

The test data used to develop the variables for the χ^2 test of track continuity can also be used to measure the resolution in invariant mass and angle α. These distributions are shown in Fig. 7. The mass resolution is characterized by a standard deviation of 2.1 MeV/c^2 and the angular resolution when fitted to a distribution $dN/d\alpha^2 = \exp(-\alpha^2/2\sigma^2)$ gives a value of σ of 1.5 mrad.

Events were considered as $K_L^0 \to \mu^+\mu^-$ or $K_L^0 \to \pi^+\pi^-$ candidates if they satisfied the following criteria:

(i) The decay vertex had to be within the beam fiducial volume. This was checked by requiring that the direction of the K_L before decay, defined by the production target and the decay vertex, be consistent with the beam divergence. Figure 8 shows the vertical-K-angle distribution for the test data along with the location of the cuts.

(2) The closest distance of approach of the two tracks at the vertex had to be within 3σ of zero. While σ was momentum dependent, the approximate position of the cut is shown in Fig. 9.

(3) The kaon momentum had to be less than 7 GeV/c, essentially the end point of the spectrum. The K_L spectrum weighted by the decay probability and the apparatus acceptance is shown in Fig. 10. This spectrum was determined by reconstruction of $K_L \to \pi\pi$ events.

(4) The cosine of the center-of-mass polar angle

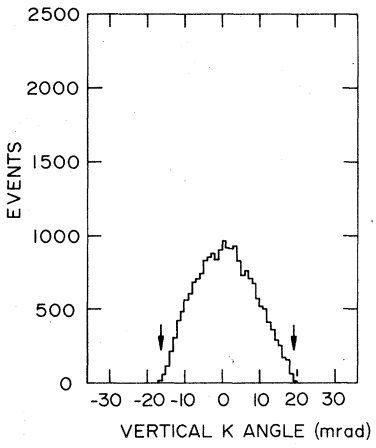

FIG. 8. Distribution in vertical angle of the K_L beam. Arrows show positions of cuts.

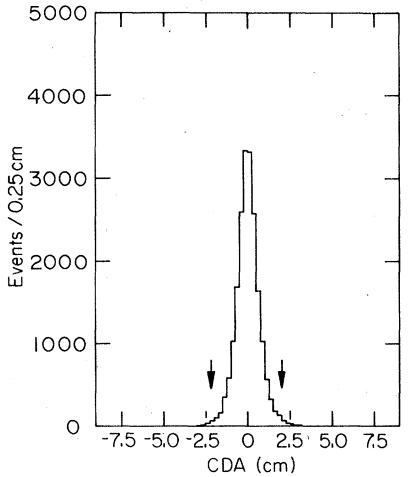

FIG. 9. Distribution of distances of closest approach at the vertex. Arrows show approximate position of cuts.

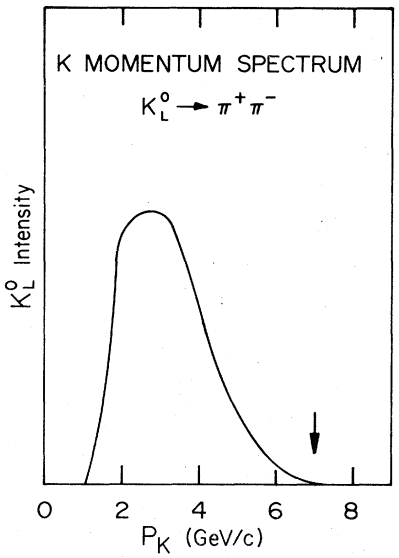

FIG. 10. Momentum spectrum of the K_L beam determined by reconstruction of $K_L \rightarrow \pi^+\pi^-$ events. Arrow shows position of the cut.

of the decay, $\cos\theta_{c.m.}$, had to be between -0.5 and $+0.5$. In the laboratory this variable becomes the relative momentum asymmetry between the positive and negative final state particles.

$$\cos\theta_{c.m.} = 1.1\,\frac{p^+ - p^-}{p^+ + p^-}\,.$$

The symmetric double-arm spectrometer configuration limited the acceptance for two-body decays to the above range. Figure 11 shows the $\cos\theta_{c.m.}$ distribution for a sample of $K_L^0 \rightarrow \pi^+\pi^-$ events.

(5) The decay vertex had to be at least 76 cm downstream of the last collimator. This requirement eliminated events which originated or scattered in the collimator. Figure 12 shows the distribution of decay vertices along the beam direction.

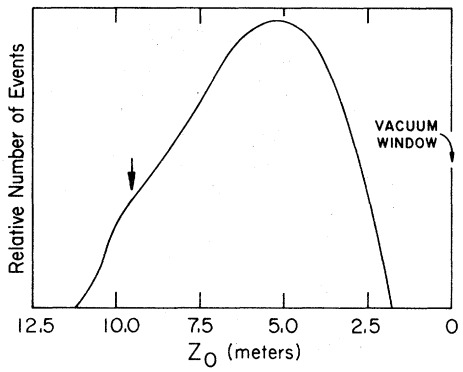

FIG. 12. Distribution of decay vertices as a function of distance from the vacuum window. Arrow shows position of the cut.

(6) In order to remove discontinuous tracks due to π decay in flight, the total χ^2 was required to be less than 20, while χ_x^2 and χ_y^2 were not permitted to exceed 14 and 18, respectively. The distributions of χ_x^2 and χ_y^2 for the test data are shown in Fig. 5; the total χ^2 distribution is shown in Fig. 13.

The effect of these cuts on good events can be seen in Table II. We have tabulated the fraction of the normalization data ($K_L^0 \rightarrow \pi^+\pi^-$) which is lost as each criterion is applied.

It is important to note that all of the above criteria were applied identically to the $K_L^0 \rightarrow \mu^+\mu^-$ candidates and to the $K_L^0 \rightarrow \pi^+\pi^-$ normalization data. The only difference in the treatment of the two data samples was the muon range requirement for the $K_L^0 \rightarrow \mu^+\mu^-$ data. The range measured by the muon identifier had to be consistent with the particle momentum. The momentum interval associated with each of the four muon counter banks was determined by studying a sample of muons from $K_L^0 \rightarrow \pi\mu\nu$ events. These events were identi-

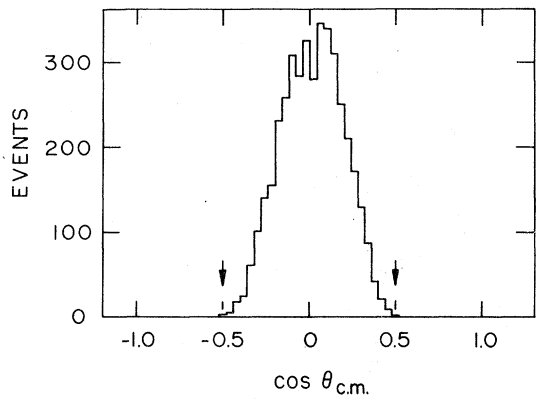

FIG. 11. Decay angular distribution of $K_L \rightarrow \pi^+\pi^-$ events. Arrows show positions of the cuts.

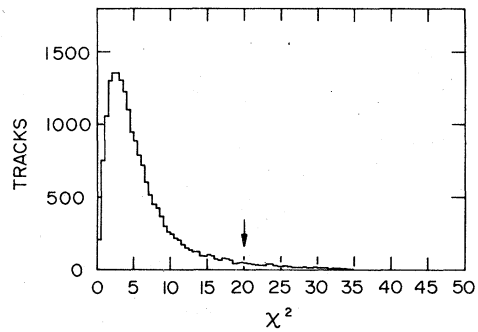

FIG. 13. Distribution of total χ^2 for continuous tracks determined from selected $K_L \rightarrow \pi^+\pi^-$ events.

TABLE II. Loss of $K_L^0 \to \pi^+\pi^-$ events due to each applied cut.

Cut	Fraction of $K_L^0 \to \pi^+\pi^-$ lost
Beam fiducial volume	0.3%
Closest distance of approach	0.5%
Kaon momentum	0.5%
$\cos\theta_{c.m.}$	0.5%
Collimator	5.6%
χ^2	10.0% (5%/track)

fied by the requirement that one particle interact (i.e., not penetrate the muon filter) and that neither particle produce a large shower-counter pulse typical of an electromagnetic shower. If the invariant mass of the particle pair was outside the region of the K_L meson mass, the second particle had to be a muon. Figure 14 shows the momentum distribution of the particles which stopped between the third and fourth gaps in the muon filter. The momentum limits thus obtained for each counter bank were further extended by $3\sigma_{straggling}$ ($\approx$100 MeV/c) in each direction. In addition, the counters which fired were required to be consistent with the horizontal and vertical track coordinates. This test was not very precise, since the counters were 12 in. wide. The requirement did nonetheless remove events in which the counters which fired were far from the particle trajectory.

The efficiency of the range requirement was measured with a sample of muons from the $K_L \to \pi\mu\nu$ events. It was found that 3% of the muons failed to satisfy the range criteria. Since there are two muons in a $K_L \to \mu^+\mu^-$ event, one must apply a 6% correction to the final branching ratio.

The electronic inefficiency for the muon trigger was found to be 2.5% ± 1%. So the total inefficiency of the $K_L \to \mu^+\mu^-$ detection with respect to the $K_L \to \pi^+\pi^-$ detection is (8.5 ± 1)%.

The $K_L \to \mu^+\mu^-$ data are shown in Fig. 15. In the region $492 \leq M_K \leq 504$ MeV/c^2 and $\alpha^2 < 7$ mrad^2 there are 16 events well separated from the background. These events have M_K and α^2 distributions which are in good agreement with those found for the $K_L \to \pi^+\pi^-$ data as shown in Fig. 16. In Fig. 17 we show a comparison of the χ^2 distribution and decay vertex distribution of the $K_L \to \mu^+\mu^-$ events with corresponding distributions for the selected $K_L \to \pi^+\pi^-$ events.

C. Estimate of $K_L \to \mu^+\mu^-$ background

We have carried out Monte Carlo calculations to evaluate the level of the expected background from $K_L \to \pi\mu\nu$. We have found it difficult to obtain agreement in exact yield between the calculation and the actual tail of the mass distribution as observed in the data. In order to be confident about the *absolute* calculated background, the Monte Carlo calculations must replicate the experimental conditions in full detail. We used empirical studies of actual trajectories in order to establish

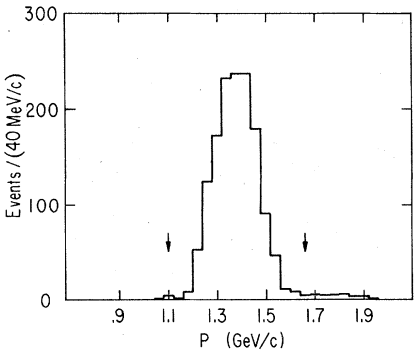

FIG. 14. Distribution of momenta of muons which stop between the third and fourth gaps in the muon filter. Arrows show positions of the cuts.

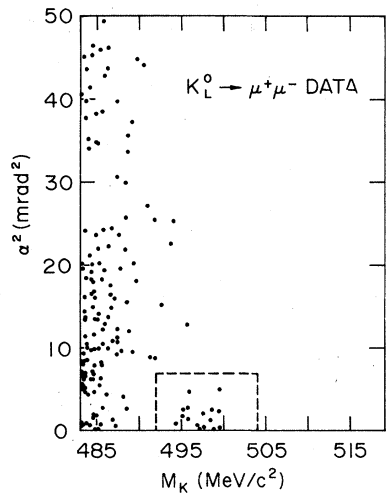

FIG. 15. Distribution of $K_L \to \mu^+\mu^-$ events in the variables M_K and α^2.

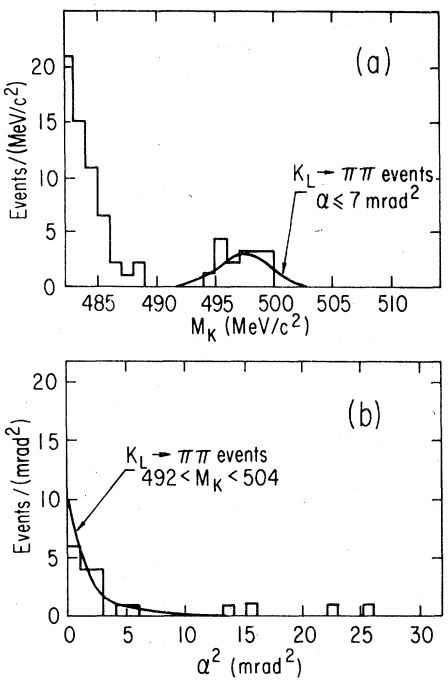

FIG. 16. (a) Comparison of the invariant-mass distribution of $K_L \to \mu^+\mu^-$ events with $\alpha^2 \leq 7$ mrad^2 to the distribution found for $K_L \to \pi^+\pi^-$ events. (b) Comparison of the α^2 distribution of $K_L \to \mu^+\mu^-$ events with $492 < M_K < 504$ (MeV/c^2) to the distribution found for $K_L \to \pi^+\pi^-$ events.

the χ^2 selection procedure, while the calculated trajectories in the Monte Carlo program used a more idealized magnetic field. However, we found that the tail in the $\mu^+\mu^-$ mass plot (with

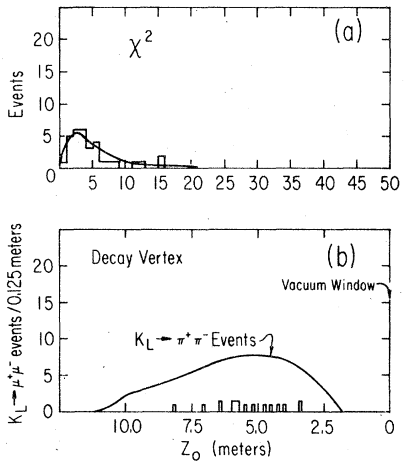

FIG. 17. (a) Comparison of the χ^2 distribution for the 16 $K_L \to \mu^+\mu^-$ events with that found for $K_L \to \pi^+\pi^-$ events. (b) Comparison of the decay vertex distribution of the $K_L \to \mu^+\mu^-$ events with that found for the $K_L \to \pi^+\pi^-$ events.

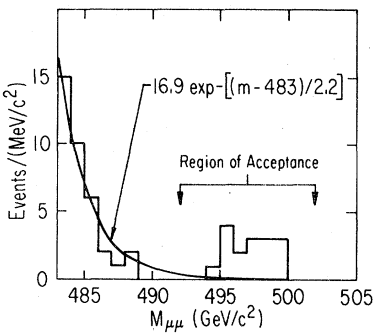

FIG. 18. Plot of calculated $K_L \to \mu^+\mu^-$ background from $K_L \to \pi\mu\nu$ superimposed on the mass plot of $K_L \to \mu^+\mu^-$ candidates.

$\alpha \leq 7$ mrad^2) was exponential and the slope constant for a wide variation of the details of the calculation. The slope agrees well with the data. Figure 18 shows the calculated $K_L \to \mu^+\mu^-$ mass distribution normalized to the data for $M_K < 490$

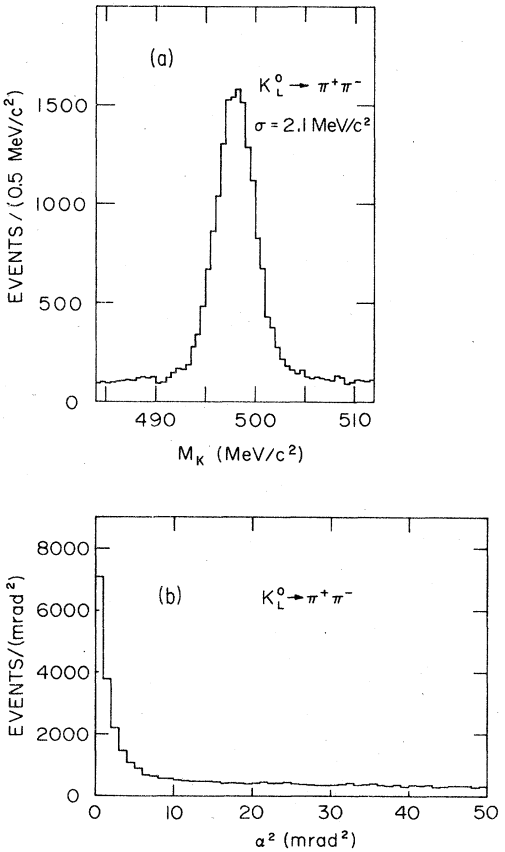

FIG. 19. (1) Number of events from $\pi^+\pi^-$ trigger with $\alpha^2 \leq 7$ mrad^2 as a function of M_K. (b) Number of events from $\pi^+\pi^-$ trigger with $492 \leq M_K \leq 504$ MeV/c^2 as a function of α^2.

MeV/c^2. If one extrapolates this curve we would expect 0.6 events due to $K_{\mu 3}$ background for $M_K > 492$ MeV/c^2. Accordingly, we subtract 0.6 events from the signal of 16 events, giving 15.4 events for the calculation of the branching ratio.

D. Selection of normalizing $K_L \to \pi^+\pi^-$ events

The events collected during the $\pi^+\pi^-$ trigger mode were treated identically to the $\mu^+\mu^-$ events except for the muon-range requirement. Unlike the selected $K_L \to \pi^+\pi^-$ events used to understand the resolution and properties of nondecaying tracks, the normalizing events had no particle identification imposed on them. A sample of events from the $\pi^+\pi^-$ trigger is shown in Fig. 19. Plotted is the mass spectrum for events with $\alpha^2 \leq 7$ mrad^2. Also plotted is a sample of the $\pi^+\pi^-$ events with $492 < M_K < 504$ MeV/c^2 as a function of α^2. Background under the mass peak was calculated using a smooth curve fit to the regions adjacent to the peak. After background subtraction, the number of $K_L \to \pi^+\pi^-$ events with $492 \leq M_K \leq 504$ MeV/c^2 and $\alpha^2 < 7$ mrad^2 in the entire data sample was found to be $29\,470 \pm 520$.

This number must be corrected for π decay in flight, since if a π decayed in the vacuum tank or spectrometer the event was lost from the M_K-α^2 peak. The correction factor was obtained directly from the $K_L \to \pi^+\pi^-$ data. Each event in the M_K-α^2 peak corresponded on the average to N $K_L \to \pi^+\pi^-$ decays in the vacuum tank, where

$$N = e^{L/\gamma\beta c\tau} e^{L/\gamma^+\beta^+ c\tau}.$$

Here L is the distance from the decay point to a point 30 cm upstream of the final spark chamber. The latter point is one downstream of which a π-μ decay cannot be discerned by the χ^2 test for track continuity. The +, − superscript refers to each of the pions in the final state. When N was calculated for all of the $K_L \to \pi^+\pi^-$ events in the selected sample we found that only 22% of the potential normalization events are lost because of π decay. Thus the corrected number of normalization events is $37\,780 \pm 670$.

Finally, in order to use this result to normalize the $K_L \to \mu^+\mu^-$ data, we have to correct for the fact that normalization data were taken during one of every sixteen accelerator pulses. In addition, the live time per pulse was considerably smaller for the normalization trigger because of the larger trigger rate. The relative exposure times for the $\mu\mu$ and $\pi\pi$ triggers were measured by the beam monitors which were gated along with the rest of the apparatus and recorded at the end of each pulse. The $\mu\mu$ exposure time for the entire experiment was 121.5 times the $\pi\pi$ exposure time. Thus, the number of normalization events appropriate to the $\mu\mu$ mode exposure was

$$N_{\pi\pi} = (4.59 \pm 0.08) \times 10^6.$$

IV. CALCULATION OF RELATIVE DETECTION EFFICIENCIES FOR $K_L \to \mu^+\mu^-$ AND $K_L \to \pi^+\pi^-$

The properties of the apparatus were extensively studied by Monte Carlo techniques. The efficiency of the apparatus for the final states $\mu^+\mu^-$, $\pi^+\pi^-$, $\pi\mu\nu$, $\pi e\nu$, and $\pi\pi\pi$ was evaluated as well as many distributions expected for each decay mode. The computer program included effects of multiple scattering, π decay in flight, measurement error, and the cuts imposed by the logic of the parallel trigger mode. The evaluation of the relative efficiency of the apparatus for $K_L \to \pi\pi$ and $K_L \to \mu\mu$ is quite insensitive to many of the details of the calculation.

The most stringent test of the Monte Carlo calculation is its ability to fit the various distributions observed. Extensive comparisons of data and Monte Carlo distributions were made in a previous publication[15] where our measurement of $\Gamma(K_L \to \pi^+\pi^-)/\Gamma(K_L \to \text{all})$ was presented. The reader is referred to this publication for further details.

The relative efficiency for $K_L \to \pi^+\pi^-$ to $K_L \to \mu^+\mu^-$ was found to be 1.10 ± 0.02. The deviation of this ratio from unity can be traced to two factors. First, for a given momentum, the opening angle of the $\mu^+\mu^-$ decay is slightly larger than the $\pi^+\pi^-$ decay, and second, for $\mu^+\mu^-$ a low-momentum cut is effectively imposed by the requirement that each muon have a momentum greater than 1050 MeV/c in order to be identified as a $\mu^+\mu^-$ event.

V. RESULT FOR $\Gamma(K_L \to \mu^+\mu^-)/\Gamma(K_L \to \pi^+\pi^-)$

The $K_L^0 \to \mu^+\mu^-$ branching rato is calculated from the equation

$$\frac{\Gamma(K_L^0 \to \mu^+\mu^-)}{\Gamma(K_L^0 \to \pi^+\pi^-)} = \frac{N_{\mu\mu}}{N_{\pi\pi}} \frac{M}{C},$$

$$N_{\mu\mu} = 15.4^{+5.1}_{-3.1} \text{ events},$$

$$N_{\pi\pi} = (4.59 \pm 0.08) \times 10^6 \text{ events}.$$

Here M is the relative acceptance of $K_L \to \pi^+\pi^-$ to $K_L \to \mu^+\mu^-$ decays. M was found to be 1.10 ± 0.02 as discussed in Sec. IV. C is a correction which is a product of two factors discussed in Sec. III: a factor 0.975 due to the measured electronic inefficiency and 0.94 due to the inefficiency of the muon range requirement. Thus,

$$\frac{\Gamma(K_L^0 \to \mu^+\mu^-)}{\Gamma(K_L^0 \to \pi^+\pi^-)} = (4.0^{+1.2}_{-0.8}) \times 10^{-6}.$$

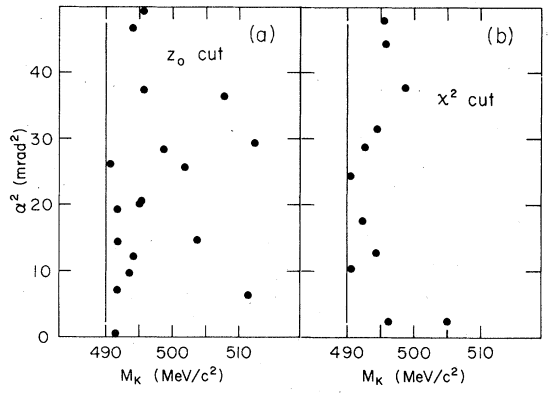

FIG. 20. (a) Additional events which appear when the collimator cut is removed. (b) Additional events which appear when the χ^2 cut is loosened to $\chi^2 < 30$.

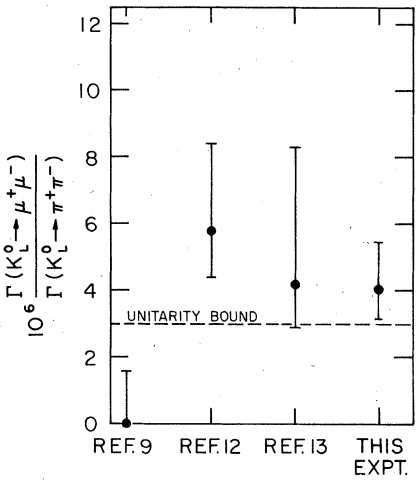

FIG. 21. Comparison of measurements of the ratio $\Gamma(K_L \to \mu^+\mu^-)/\Gamma(K_L \to \text{all})$. All error bars are one standard deviation except for Ref. 9 which is at the 90% confidence limit.

Two of the event-selection criteria removed more than 1% of the normalization data: the collimator cut and the χ^2 cut. Figure 20 shows the *additional* $\mu^+\mu^-$ events with $M_K > 490$ MeV/c^2 when these criteria are *significantly* loosened. If events with decay vertices near and even within the last collimator are accepted, the background increases substantially [Fig. 20(a)]. If the χ^2 requirement is relaxed to $\chi^2 < 30$, then one additional event inside the region of the M_K-α^2 peak appears along with many additional background events [Fig. 20(b)].

We have calculated the effect on the result due to changes in all the event selection criteria. The position of each cut was moved by 10% in each direction. In every case except three, the result changed by less than 1%. A reduction in the vertical size of the beam fiducial volume reduced the result by 3%. An increase in the $\cos\theta_{\text{c.m.}}$ cut increased the result by 5%. Finally, a 4% increase resulted from the increase in the χ^2 cut. These variations are all small compared to the statistical uncertainty. Folding in these uncertainties gives the final result

$$\frac{\Gamma(K_L^0 \to \mu^+\mu^-)}{\Gamma(K_L^0 \to \pi^+\pi^-)} = (4.0^{+1.4}_{-0.9}) \times 10^{-6}.$$

The errors are one standard deviation.

We have also measured with the same apparatus the quantity $\Gamma(K_L \to \pi^+\pi^-)/\Gamma(K_L \to \text{all})$ (Ref. 15) and find it to be $(2.01 \pm 0.09) \times 10^{-3}$. Using this value we find

$$\frac{\Gamma(K_L \to \mu^+\mu^-)}{\Gamma(K_L \to \text{all})} = (8.1^{+2.8}_{-1.8}) \times 10^{-9}.$$

Our result is compared with those previously obtained for this ratio in Fig. 21. The three most recent experiments are consistent with the ratio and are above the unitarity bound.

Conclusive evidence exists for the process $K_L \to \mu^+\mu^-$ and its magnitude presents no contradiction to fundamental theoretical principles. There is, however, no evidence for a strangeness-changing weak neutral-current interaction since the rate is entirely consistent with the rate predicted from $K_L \to \gamma\gamma$ and quantum electrodynamics.

ACKNOWLEDGMENTS

We would like to thank the staff of the Argonne ZGS for their help during the construction and operation of the experiment. Electronics support was provided by T. Nunamaker and the staff of the electronics development group at the University of Chicago. Sollie Lucero provided much of the mechanical design, and the engineering service group aided in the construction of the apparatus. We also thank G. Gusik, G. Henry, A. Crawford, D. Antreasyan, N. Thalassinos, and C. Shaw, who helped during various stages of the experiment. One of us (J.W.C.) acknowledges the hospitatlity of the Aspen Center for Physics where the final version of this paper was prepared. This research was supported by the National Science Foundation and the U.S. Energy Research and Development Administration.

*Present address: Department of Physics, California Institute of Technology, Pasadena, California 91125.
†Present address: IBM Corporation, San Jose, California 95193

[1]H. Foeth *et al.*, Phys. Lett. 30B, 282 (1969).
[2]P. Darriulat *et al.*, Phys. Lett. 33B, 249 (1970).
[3]S. M. Berman and D. A. Geffen, Nuovo Cimento 18, 1192 (1960).
[4]D. A. Geffen and B. L. Young, Phys. Rev. Lett. 15, 316 (1965).
[5]C. Quigg and J. D. Jackson, Lawrence Radiation Laboratory Report No. UCRL 18487, 1968 (unpublished).
[6]L. M. Sehgal, Phys. Rev. 183, 1511 (1969).
[7]B. R. Martin, E. de Rafael, and J. Smith, Phys. Rev. D 2, 179 (1970).
[8]Particle Data Group, Rev. Mod. Phys. 48, S 1 (1976).
[9]A. R. Clark *et al.*, Phys. Rev. Lett. 26, 1667 (1971).
The experimental upper limit has since been increased to 3×10^{-9}. This is due to the change in the accepted value for $\Gamma(K_L\to\pi^+\pi^-)/\Gamma(K_L\to\text{all})$ as well as a recalculation of the $K_L\to\pi^+\pi^-$ and $K_L\to\mu^+\mu^-$ acceptances. R. C. Field, SLAC Report No. SLAC-PUB-1498, 1974 (unpublished).
[10]H. Stern and M. K. Gaillard, Ann. Phys. (N. Y.) 76, 580 (1973).
[11]A. D. Dolgov, L. B. Okun, and V. I. Zakharov, ITEP Report No. 924, Moscow, 1972 (unpublished).
[12]W. C. Carithers *et al.*, Phys. Rev. Lett. 30, 1336 (1973); W. C. Carithers *et al.*, *ibid.* 31, 1025 (1973).
[13]Y. Fukushima *et al.*, Phys. Rev. Lett. 36, 348 (1976).
[14]M. J. Shochet *et al.*, Phys. Rev. Lett. 39, 59 (1977).
[15]R. DeVoe *et al.*, Phys. Rev. D 16, 565 (1977).
[16]D. Ayres and R. Diebold, private communication.
[17]T. A. Nunamaker, Rev. Sci. Instrum. 42, 1701 (1971).